Initial Results of Rover Localization and Topographic Mapping for the 2003 Mars Exploration Rover Mission

Rongxing Li, Steven W. Squyres, Raymond E. Arvidson, Brent A. Archinal, Jim Bell, Yang Cheng, Larry Crumpler, David J. Des Marais, Kaichang Di, Todd A. Ely, Matt Golombek, Eric Graat, John Grant, Joe Guinn, Andrew Johnson, Ron Greeley, Randolph L. Kirk, Mark Maimone, Larry H. Matthies, Mike Malin, Tim Parker, Mike Sims, Larry A. Soderblom, Shane Thompson, Jue Wang, Patrick Whelley, and Fengliang Xu

Abstract

This paper presents the initial results of lander and rover localization and topographic mapping of the MER 2003 mission (by Sol 225 for Spirit and Sol 206 for Opportunity). The Spirit rover has traversed a distance of 3.2 km (actual distance traveled instead of odometry) and Opportunity at 1.2 km. We localized the landers in the Gusev Crater and on the Meridiani Planum using two-way Doppler radio positioning technology and cartographic triangulations through landmarks visible in both orbital and ground images. Additional high-resolution orbital images were taken to verify the determined lander positions. Visual odometry and bundle-adjustment technologies were applied to overcome wheel slippages, azimuthal angle drift and other navigation errors (as large as 21 percent). We generated timely topographic products including 68 orthophoto maps and 3D Digital Terrain Models, eight horizontal rover traverse maps, vertical traverse profiles up to Sol 214 for Spirit and Sol 62 for Opportunity, and five 3D crater models. A web-based landing-site Geographic Information System (GIS) has been set up at The Ohio State University to update and disseminate the daily localization and topographic information to support tactical and strategic operations of the mission. Also described in this paper are applications of the data for science operations planning, geological traverse survey, survey of wind-related features, and other science applications. The majority of the instruments onboard both rovers are healthy at this moment, and they will continue to explore the two landing sites on the Martian surface. We expect to report further localization and topographic mapping results to be achieved in the rest of the mission period and in post-mission data processing.

Introduction

Spirit (MER-A) and Opportunity (MER-B) rovers carrying identical science and engineering instrument payloads (Figure 1) are exploring the landing sites of Gusev Crater and Meridiani Planum on the Martian surface (Squyres *et al.*, 2003; 2004a; 2004b). A detailed description of the MER rover sensors and key parameters relevant to topographic mapping and rover localization is given in Li *et al.* (2004a). Pancam (panoramic camera) and Navcam (navigation camera) are the most important imaging systems for our localization and mapping research activities. These two stereo imaging systems are mounted on the same camera bar of the rover mast. The imaging areas of both Pancam and Navcam are 1,024 pixels × 1,024 pixels. Navcam has a stereo base of 20 cm, a focal length of 14.67 mm, and an effective depth of field of 0.5 meters to infinity. Its best focus is at 1 m with a field of view (FOV) of 45 degrees. Pancam has a wider stereo base (30 cm) and a longer focal length (43 mm), making it more effective in mapping medium-to-far objects in panoramic images. The effective depth of field for the Pancam is 3 meters to infinity and FOV is 16 degrees.

Localization of Spirit and Opportunity is of fundamental importance to understanding where the vehicles have traversed and how to get the rovers to new locations (Arvidson *et al.*, 2004). The mission has focused on traversing

Rongxing Li, Kaichang Di, Jue Wang, and Fengliang Xu are with the Department of Civil and Environmental Engineering and Geodetic Science, The Ohio State University, Columbus, OH 43210 (li282@osu.edu).

Steven W. Squyres and Jim Bell are at Cornell University, Ithaca, NY.

Raymond E. Arvidson is at Washington University, St. Louis, MO.

Yang Cheng, Todd A. Ely, Matt Golombek, Eric Graat, Joe Guinn, Andrew Johnson, Mark Maimone, Larry H. Matthies, and Tim Parker are with the Jet Propulsion Laboratory, Pasadena, CA.

Larry Crumpler is with the New Mexico Museum of atural History and Science, Albuquerque, NM.

David J. Des Marais and Mike Sims are with the Ames Research Center, Moffett Field, CA.

John Grant is with the Smithsonian Institution, Washington, D.C.

Ron Greeley, Shane Thompson, and Patrick Whelley are with Arizona State University, Tempe, AZ.

Brent A. Archinal, Randolph L. Kirk, and Larry A. Soderblom are with the U.S. Geological Survey, Flagstaff, AZ.

Mike Malin is with Malin Space Science Systems, San Diego, CA.

Photogrammetric Engineering & Remote Sensing
Vol. 71, No. 10, October 2005, pp. 1129–1142.

0099-1112/05/7110–1129/$3.00/0

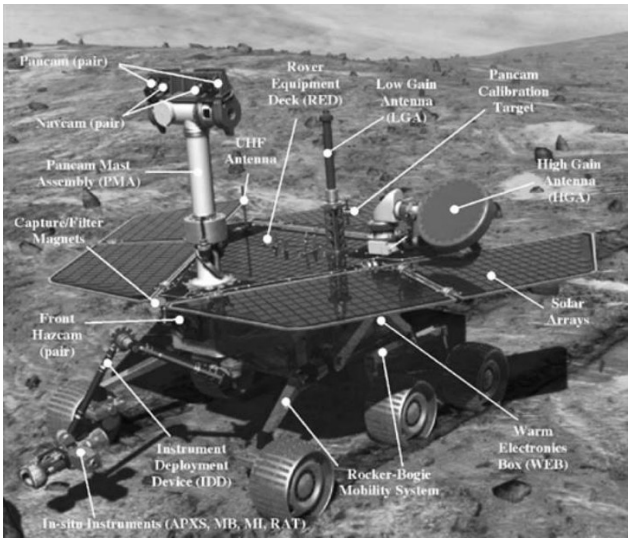

Figure 1. MER rover with science and engineering payload instruments.

to key terrains, soil deposits, rock fields, and outcrops. Remote sensing observations using the Pancam and Mini-TES systems were used to identify key targets for detailed study. The rovers were then commanded to traverse to these targets, with fine-scale positioning used to place the vehicles in locations where the instrument deployment devices (IDD) could be used to place the Mössbauer Spectrometer (MB), Alpha Particle X-Ray Spectrometer (APXS), Microscopic Imager (MI), or Rock Abrasion Tool (RAT) tools onto surfaces for acquisition of *in situ* observations, and in the case of the RAT, to first brush or grind away surface covers. All of these operations demanded accurate three-dimensional location information. Furthermore, localization for traverses and conversion to the Mars inertial and Mars body-fixed (MBF) coordinate systems (Li *et al.*, 2004a) were necessary to be able to place rover-based observations in a regional scale context seen, for example, from orbital imagery.

Each rover's onboard navigation system consists mainly of an Inertial Measurement Unit (IMU), an odometer, and the Pancam used as a solar imaging camera. Rover positions, image-pointing parameters, and camera models were delivered as telemetry information in separate files as well as in image headers. The JPL Multimission Image Processing Laboratory (MIPL) produced mosaics, linearized (epipolar) images, range maps, and other products within a few hours after downlink (or within one Martian day, or "sol") to support rover navigation and science operations. The Science Activity Planner (SAP) system developed by the JPL Web Interface for Telescience (WITS) is a very effective tool for the science team members, allowing them to use downlinked images, range maps, mosaics, and measuring functions for various science-oriented operations and for building high-level, day-to-day rover operation sequences (Norris *et al.*, 2004).

Orbital images were available pre- and post-landing. Pre-landing images included those obtained from the Viking vidicon camera that takes images of approximately 200 meters/pixel, the Odyssey Thermal Emission Imaging System (THEMIS) that includes a visible channel with a resolution of 18 m, and an infra-red channel with a resolution of 100 m, and the Mars Global Surveyor (MGS), Mars Orbiter Camera (MOC) that has an narrow angle (NA) mode of 1.5 to 3 meters and a wide angle (WA) mode with a basic resolution of 248 m (230 m in digital products at 256 pixels/degree). Post landing, MGS took additional MOC compensated Pitch and Roll Targeted Observation (cPROTO) and Roll-Only Targeted Observation (ROTO) images of the landing sites with a resolution of 1 m. Most topographic products derived from the orbital images, such as the U.S. Geological Survey (USGS) Mars Digital Image Mosaic (MDIM 2.1), are referenced to the MBF reference system. The best accuracy achieved by such orbital data-derived maps is about 100 m (Li *et al.*, 2004a). For each landing site, three Descent Image Motion Estimation System (DIMES) sequential images were taken at about 1,000 m during the descending process for the purpose of safe landing; these can be used for lander localization and regional topographic mapping. The orbiter-to-ground linkage can be accomplished by cross-correlating features observed on ground images acquired from the rovers with features observed in descent and orbital images.

This paper presents the initial results of lander and rover localization and topographic mapping of the MER 2003 mission (by Sol 225 for Spirit and Sol 206 for Opportunity). At that time, the Spirit rover had traversed a distance of 3.2 km (actual distance traveled instead of odometry) and Opportunity 1.2 km. We localized the landers in the Gusev Crater and on the Meridiani Planum using two-way Doppler radio positioning technology and cartographic triangulations through landmarks visible in both orbital and ground images. Additional high-resolution orbital images were taken to verify the determined lander positions. Visual-odometry (VO) and bundle-adjustment (BA) technologies were applied to overcome wheel slippages, azimuthal angle drift, and other navigation errors, and provide accurate rover traverse information. Various topographic products were generated routinely. A web-based landing-site GIS system has been set up at The Ohio State University (OSU) to update and disseminate the localization and topographic information as frequently as daily in support of the mission's tactical and strategic operations. Also given in this paper are applications of the data for science operations planning and for other geological applications.

Localization of Landers

Determining where each lander is located in the Mars global reference system (either the inertial reference system or MBF) and with respect to other surface features in the landing site local (LSL) reference system (Li *et al.*, 2004a) as soon as possible after landing was critical for planning science and engineering activities in the initial stages of rover exploration and for identifying other nearby features to plan long-range rover traverses over the course of the mission. Initial localization was accomplished for both landers within eight days of landing (before the rovers began moving). This activity involved tracking the communications link in the inertial reference frame; reconstructing the entry, descent and landing (EDL) in returned DIMES descent images and locating common features in the lander and orbiter images in the MBF and LSL reference systems.

On 04 January 2004, the Spirit rover landed in Gusev Crater about 12 km east of the center of a landing ellipse that had major and minor axes of 78 km and 10 km, respectively. The navigation team determined the location of the lander through fitting direct-to-earth (DTE) two-way X-band Doppler signals from Sol 2 to Sol 4 and two passes of UHF two-way Doppler signals between Spirit and the Mars Odyssey orbiter. The Spirit lander location was determined in the inertial space and translated to the MBF system (MOLA IAU 2000) as 14.571892°S, 175.47848°E (Guinn and Ely, 2004;

Golombek and Parker, 2004). Starting Sol 1, when the first Navcam panorama was acquired, careful correlations have been made of ground features such as hills and craters in both the lander panoramas and the DIMES descent and MOC images. The optimal cartographic triangulation resulted in the location 14.5692°S, 175.4729°E (Golombek and Parker, 2004; Parker *et al.*, 2004). The Nav radio-tracking solution and optimal cartographic triangulation results are shown in Figure 2. This lander location was later unofficially named "Columbia Memorial Station."

Twenty-one days later, on 25 January, the Opportunity rover landed on Meridiani Planum. The location of the Opportunity lander in the inertial reference system was determined by fitting DTE two-way X-band Doppler radio transmissions and two passes of UHF two-way Doppler between the Opportunity rover and the Mars Odyssey orbiter. Translated to the MBF system, the lander was located at 1.948282°S, 354.47417°E (Guinn and Ely, 2004; Golombek and Parker, 2004). The first Navcam panorama taken on Sol 1 indicated that the spacecraft landed in a crater. However, a number of craters appeared in the navigation solution of the surrounding area. To determine the exact crater of landing, a 3D crater model was generated using a three-tiered Pancam panorama. Crater parameters such as rim size, shape, and texture patterns were used to compare the craters appearing on the DIMES images with the 3D crater model and the ground images (Li *et al.*, 2004b). EDL reconstruction data were examined for the same purpose (Johnson, personal communication, 2004). The location of the lander at 1.9462°S, 354.4734°E was determined using triangulation to three craters observed in the far field (through breaks in the local crater rim) in both the lander panorama and the DIMES descent and MOC NA images (Golombek and Parker, 2004; Parker *et al.*, 2004). The lander location, Nav radio-tracking solution, and other localization features are shown in Figure 3. This lander location was later nicknamed "Eagle Crater."

Figure 4a shows the location of the Spirit rover after landing and at the software upload on Sols 94 through 98, south of Bonneville Crater. The locations to the northwest were determined using triangulation to surface features visible in the orbital MOC and descent DIMES images. The navigation team determined the locations to the southeast (marked inertial) by fitting direct-to-earth two-way X-band Doppler radio transmissions and two passes of UHF two-way Doppler between Spirit and Mars Odyssey at the landing site and by two passes of UHF two-way Doppler between Spirit and Mars Odyssey at the software upload spot.

Similarly, Figure 4b shows the location of the Opportunity rover after landing and at software upload on Sols 75 through 78 in the Anatolia region. The locations to the north-northwest were determined using triangulation to surface features visible in the orbital MOC and descent DIMES

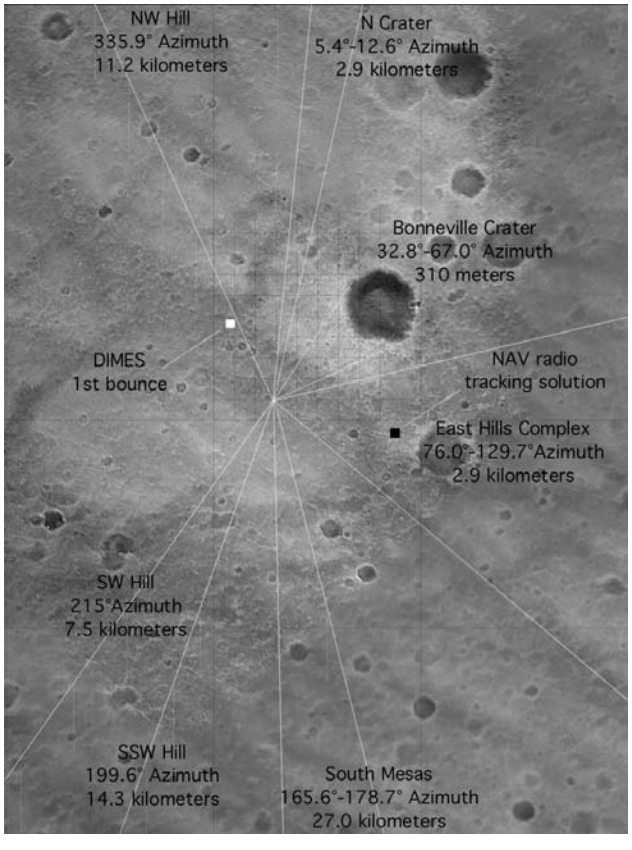

Figure 2. Spirit lander localization: High-resolution DIMES and MOC mosaic of area around the Spirit lander. Black square shows the location of the navigation solution described in the text. White square shows the first bounce point from the DIMES EDL reconstruction. Lines show azimuths to crater rims and hills clearly visible from the Spirit lander.

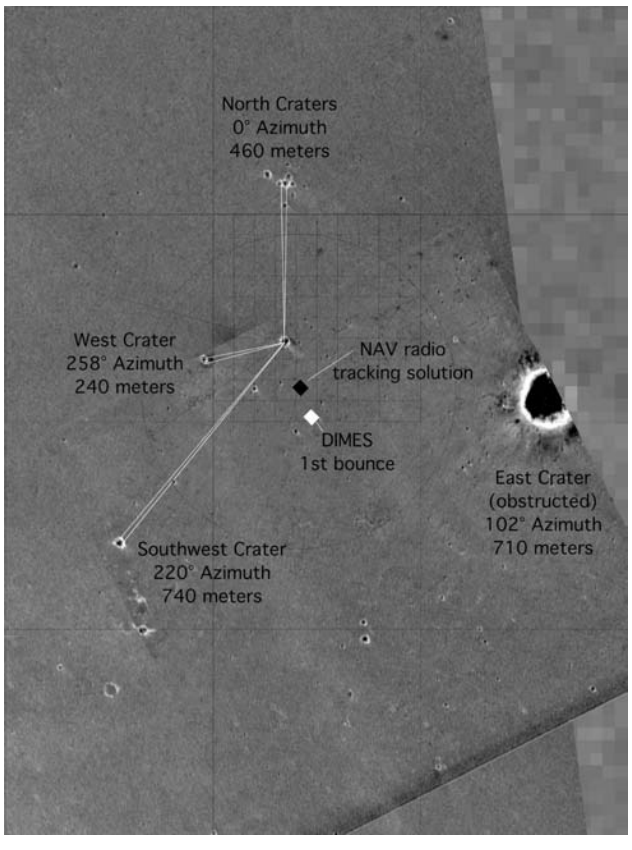

Figure 3. Opportunity lander location: High-resolution DIMES and MOC mosaic of area around the Opportunity lander. Black square shows the location of the navigation solution described in the text. White square shows the first bounce point from the DIMES EDL reconstruction. Lines show azimuths to crater rims clearly visible from the Opportunity lander.

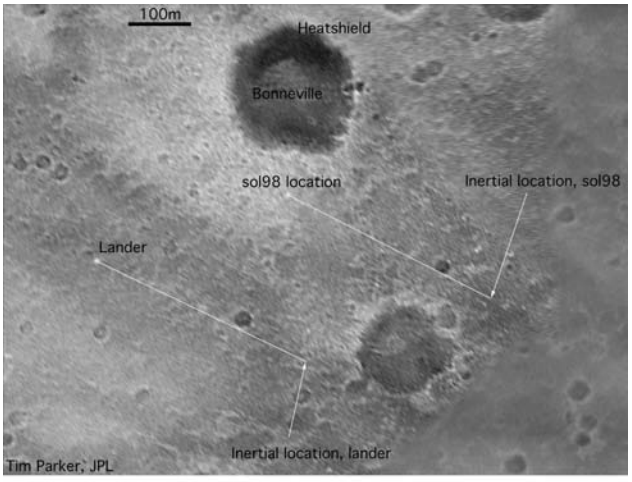

(a)

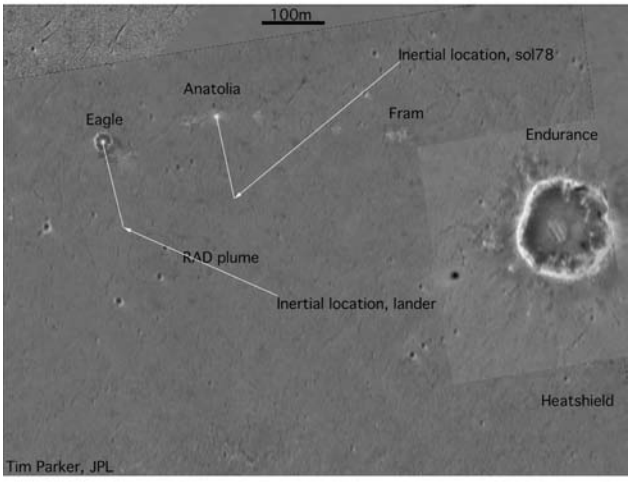

(b)

Figure 4. Rover locations determined by cartographic triangulation and radio science based on navigation techniques at the lander positions and the software upload locations as well as their offset vectors at the (a) Gusev Crater site and (b) Meridiani Planum site.

images. The navigation team determined the locations to the south-southeast (marked inertial) by fitting direct-to-earth two-way X-band Doppler radio transmissions and two passes of UHF two-way Doppler between Opportunity and Mars Odyssey at the landing site and by two passes of UHF two-way Doppler between Opportunity and Mars Odyssey at the software upload spot.

In the MOLA IAU 2000 cartographic reference frame (Li *et al.*, 2004a; Golombek and Parker, 2004), the Spirit rover at software upload was located at 14.5673°S, 175.4779°E (Figure 4a). In inertial space translated to the MOLA IAU 2000 frame, the Spirit rover at software upload was located at 14.570105°S, 175.48345°E. At landing, the inertial location was displaced to the southeast by 370 m at an azimuth of 116 degrees. At software upload, the inertial location was displaced to the southeast by 360 m at an azimuth of 117 degrees. Similarly, in the MOLA IAU 2000 cartographic reference frame the Opportunity rover at software upload was located at 1.9453°S, 354.4766°E (Figure 4b). In inertial space translated to the MOLA IAU 2000 frame, the Opportunity rover at software upload was located at 1.9475160°S, 354.47716°E. At landing and at software upload, the inertial locations were displaced to the south-southeast by 135 m at an azimuth of 167 degrees. These displacements are marked by thin lines on Figures 4a and 4b. The fact that the offset is so similar in azimuth and distance at the two locations within each site suggests that both the inertial and cartographic localization techniques are robust and accurate and no unaccounted for random errors exist in either. The observed systematic offset is most likely an offset between the cartographic frame and the inertial frame and the observed offset is close to the 3 sigma estimate found in pre-landing maps (Golombek and Parker, 2004).

Navigation solutions are useful, for example, for applications related to the Mars Odyssey or MGS orbiters and the Deep Space Network (DSN). On the other hand, cartographic solutions can be used for applications that refer to a map or to the locations of the landers with respect to other surface features. The MOC NA orbiter imager aimed itself at the two estimated lander locations and took a new, high-resolution (1 m) CPROTO image at the Gusev Site on Sol 16 and a ROTO image at the Meridiani Site on Sol 8 (Malin, 2004). Using the MOC NA images before landing and the MOC CPROTO and ROTO images after landing, the locations of the landers were verified through changes in pixels (mainly contributed by the reflection of solar panels).

Rover Localization

Rover localization has been conducted at several levels (Li *et al.*, 2004a). Within each sol cycle, the onboard IMU and wheel odometry-based localization was regularly performed with infrequent support from sun-finding techniques that improve the quality of the azimuth. In cases where the rover experiences slippage caused by traversing on loose soil terrain or against steep slopes (particularly when in craters) the onboard visual odometry (VO) technique was applied. VO is also used whenever a highly accurate rover position is desirable. In general, VO acquires consecutive Navcam stereo pairs within a traverse segment between two rover locations when Navcam or Pancam panoramas were often taken on separate sols. Finally, the bundle-adjustment (BA) technique was used to build an image network containing all panorama and traversing images (along with any available VO results) to achieve a highly accurate localization of rover positions along the entire traverse. BA was conducted on the ground (Earth).

Visual Odometry

The MER rovers update their onboard estimate of rover position and orientation at 8 Hz. Changes in attitude (roll, pitch, and yaw) are measured using a Litton LN-200 IMU that has three-axis accelerometers and three-axis angular rate sensors. Changes in position are estimated based on the IMU data and how much the wheels have turned (wheel odometry). Both blind and autonomous drive motion is typically based on simple primitive operations: straight line drives, curved arcs, or turns in place (Biesiadecki and Maimone, 2005).

In between primitive operations, the rover can make use of camera-based visual odometry to correct any errors in the initial wheel odometry-based estimate that occur when the wheels lose traction, for example, on large rocks and steep slopes. The VO system computes an update to the rover pose (x, y, z, i.e., roll, pitch, yaw) by tracking the motion of "interesting" terrain features between two consecutive pairs of stereo images in both 2D pixel coordinates and 3D ground coordinates.

Potential interesting features are identified in the first left image using the Förstner interest operator; a subset that

spans the complete image is selected. Interesting features in this subset are then projected into the second left image and matched using correlation. Several consistency checks are applied to filter out incorrect matches, including 3D ray gap analysis, a rigidity check and an iterative Random Sample Consensus (RANSAC) process. Finally, a maximum likelihood estimator is applied to the computed 3D offsets to produce the final motion estimate. However, if any one of the consistency checks fails, too few feature points are detected, or the estimation procedure fails to converge, then no motion estimate update will be produced and the initial estimate (based on wheel odometry) will be maintained. A more detailed description of this algorithm can be found in Olson *et al.* (2003) and Li *et al.* (2004a).

Visual odometry processing was performed on both MER rovers using mast-mounted Navcam imagery. To ensure that enough features can be tracked, at least 60 percent overlap between adjacent images was recommended; therefore all visual odometry drives were split into several small steps. During each step the rover was typically commanded to drive no more than 75 cm in a straight line or curved arc and, when turning in place, was commanded to change heading by no more than 18 degrees per step. Although visual odometry processing could have been beneficial during all rover motion, each step required over two minutes of processing time on MER's 20 MHz RAD6000 CPU. Therefore, it was only commanded during relatively short drives (less than 10 m) that occurred either on steep slopes (typically more than 10 degrees), or in situations where a wheel was being dragged (digging a trench or conserving drive motor lifetime on Spirit's right front wheel). The onboard IMU exhibited a very small drift rate (usually less than three degrees per hour of operation) and maintained attitude knowledge very well. Therefore, from January through August 2004, only visual odometry was typically used to update rover positions.

On Opportunity, visual odometry computation converged to a solution 231 out of 274 times within 39 sols. On Spirit, VO converged to a solution 83 of 103 tries in 12 sols as of September 2004. Table 1 summarizes the visual odometry results at the two sites. Instances where it failed to converge are primarily attributable to either too large a motion (e.g., commanding a 40 degree turn in place which resulted in too little image overlap) or lack of interesting features in the imaged terrain. VO successfully measured slips as high as 125 percent (on Sol 206 when Spirit tried to drive up more than a 25 degree slope). The longest drives using VO were 9.6 m on Sol 208 and 6.9 m on Sol 184 for Spirit and Opportunity, respectively.

Figure 5 shows two views of a sample trajectory taken by Opportunity during Sols 188 through 191. The rover was driven uphill and across slope over a total actual distance of 19 m, but wheel odometry underestimated the distance by 1.6 m. The course on the right indicates the course estimated by the wheel odometry subsystem; the course on the left shows the visual-odometry-corrected course plot. The final positions differ by nearly 5 m.

Consequently, several benefits were realized by the use of visual odometry. Science observations requiring precision pointing were often scheduled in the middle of drives; visual odometry helped to ensure accurate data collection. The accuracy of driving in new or mixed-soil terrains was improved by re-pointing to the drive goal or re-computing the distance remaining to the goal after each step along the way. Lastly, it also supplied high quality initial pointing data for the subsequent bundle adjustment data processing.

TABLE 1. STATISTICS OF VISUAL ODOMETRY RESULTS

	MER-A 64 Forward Arcs	MER-B 111 Forward Arcs
	Mean	Mean
Commanded Distance (m)	0.63	0.45
Position Change (m)	0.18	0.12
Radial Slip (%)	30	27

Incremental Bundle Adjustment

Images used in bundle adjustment (BA) are linearized (epipolar) images with practically no y parallax. The CAHV camera model (Di and Li, 2004), which is defined in the rover frame, is included in the image header. To facilitate rover operations in an extended landing site, individual site frames are defined along the traverse. The position and attitude of each rover frame with respect to its site frame is defined by three translations and a set of quaternion parameters, which are also included in the image header. The first site frame

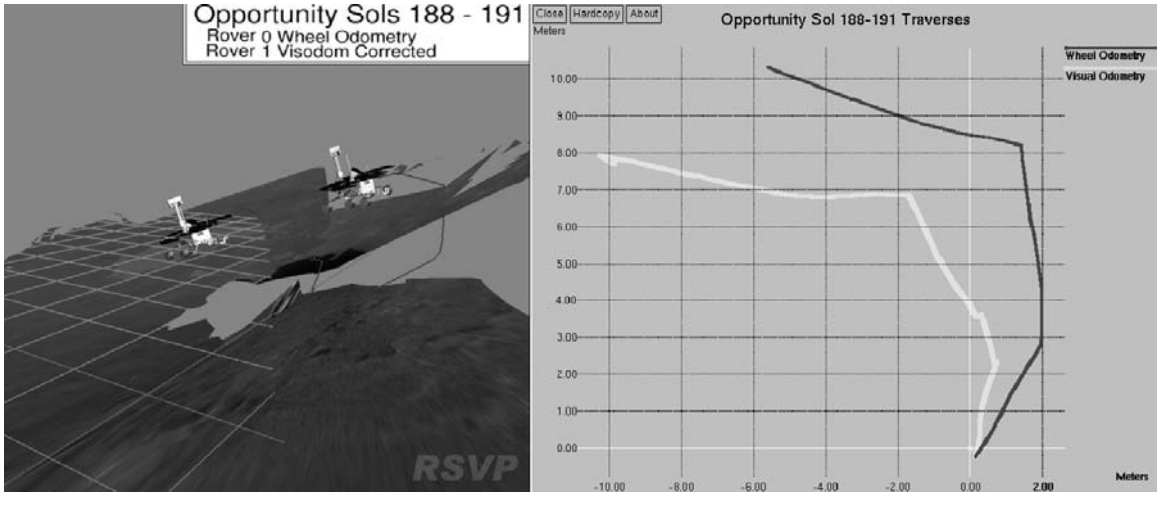

Figure 5. Two views of a sample trajectory correction by visual odometry. The trajectory was taken by Opportunity during Sols 188 through 191.

(Site 0), which is at the lander, is defined as the LSL frame for mapping and rover localization purposes. The relative positions of other site frames to the LSL are stored in a master file. We first convert the CAHV camera model to a photogrammetric model that is necessary for BA and is commonly used in topographic mapping and remote sensing (Di and Li, 2004). The camera model is then transformed in the site frame and subsequently in the LSL. Such information originates from telemetry data and is used as initial information in the bundle adjustment. Whenever VO is performed, its result is automatically supplied within the image header and also used as initial information in the bundle adjustment.

As depicted in Figure 6, Pancam and Navcam panoramas and traversing stereo images were taken at different locations. The Pancam panoramas were acquired mainly at locations where substantial science exploration activities took place, while Navcam panoramas were taken more frequently for navigation and near-rover site characterization. They were also employed to establish new site frames. Within each site frame, rover positions are determined locally. Traversing images include downlinked VO images, middle point survey images, and other images taken at each end of traverse segments. These images are linked together by tie points to form a continuous image network along the rover traverse. The purpose of BA of the image network is to optimally (in a least-squares sense) adjust the pointing parameters (camera center position and three rotation angles) of each image in the network as well as to adjust the 3D positions of the tie points. In this way, BA provides optimal rover positions at the times when the images were taken. A new incremental bundle-adjustment method was developed (Li *et al.*, 2002; 2004a) and employed to perform sol-by-sol BA operations for both rovers.

The success of bundle adjustment depends heavily on the tie points that are used to connect the rover images. In order to build a geometrically strong image network, a sufficient number of well-distributed tie points must be extracted and selected to link all the images processed. We developed a method that can automatically extract tie points from the intra-stereo and inter-stereo panoramic Navcam and Pancam images (Xu *et al.*, 2002; Di *et al.*, 2002; Li *et al.*, 2003). In a typical Navcam and Pancam panorama, over 90 percent of the tie points can be selected automatically. During the MER mission operations, this automation process greatly reduced the amount of tedious manual tie-point selection work and accelerated the rover localization and map production process. However, selection of cross-site tie points (tie points between images taken in different site frames) remains a very challenging task and is currently done manually.

Pointing information of images from telemetry data within one panorama is generally consistent. However, that of images taken in adjacent site frames often shows inconsistencies caused by wheel slippages and other navigation errors. Since the inconsistencies between adjacent site frames appeared to be systematic, we always applied a transformation (translation and rotation without scale change) to the last site frame based on cross-site tie points to ensure that better initial pointing information of the BA network is achieved for convergence.

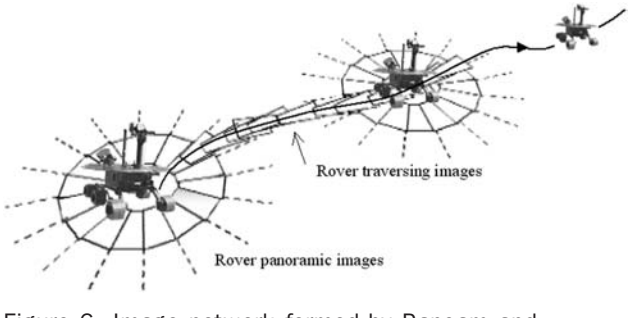

Figure 6. Image network formed by Pancam and Navcam panoramic and traversing images.

Images appropriate for BA have been collected for the Gusev Crater landing site. Post-drive panoramas (from Navcam, and occasionally Pancam) or 3 × 1 (3 columns by 1 row) mosaics in the driving direction were collected for site characterization and rover navigation. During long drives (for example, over 60 meters) a middle point survey (four Navcam images separated by 45 degrees) or rear-looking Pancam observation (3 × 1) was commanded at the end of the drive. Bundle adjustment of the rover traverse was performed at regular intervals (Plate 1d). Figure 7 shows the Spirit rover traverse up to Sol 100. The line with triangular points is the traverse generated from telemetry, while the line with circular points is the bundle-adjusted traverse. The sol numbers are also shown on the map. At the end of the traverse, the accumulated difference between these two traverses is 11.5 m, or 2 percent of the traveled distance from the landing center, with a maximum of 12 m (2 percent) on Sol 100.

For the Meridiani Planum Site, we conducted BA within the Eagle Crater (up to Sol 62). Figure 8 shows the Opportunity rover traverse up to Sol 62. The accumulated difference reached 20.2 m, or 20.5 percent of the traveled distance, with a maximum of 21 m (13 percent) on Sol 62. Significant localization errors in the telemetry data were mainly caused by wheel slippage when Opportunity encountered loose soil on the steep crater wall for 56 sols during its traverse. The BA traverse was able to correct these significant localization errors and put images and observations in context, as well as support science planning and other applications.

On the way from Eagle Crater to the Anatolia region, there is a data gap for a distance of about 100 m that makes a bundle adjustment-based traverse impossible. To continue tracking the rover's global positions, new traverse segments after the gap were computed from telemetry without BA. These were connected to the end of the bundle-adjusted traverse. By doing so, large features such as the Fram and Endurance Craters, when measured from the ground images along the traverse, are generally well matched with their positions on the MOC NA image. This indicates that the rover did not experience significant slippages after exiting Eagle Crater, as it had within Eagle Crater. However, with Opportunity's busy activities on the crater wall and near the bottom in the dune field inside Endurance Crater, significant slippages again occurred. An orthophoto map-based traverse adjustment was used to correct these errors. An orthophoto map of the entire Endurance Crater was generated using two Pancam panoramas taken at the crater rim (see Figure 12a). This orthophoto map was used as a base map for this adjustment. After the rover entered the crater, comparisons were made between features in orthophoto images (made using telemetry data at various rover locations) and the base orthophoto map. The matched features allowed us to correct the traverse in an effective way. This adjustment method enabled us to provide the Opportunity traverse in a timely manner. A separate bundle adjustment of the second part of the traverse is planned.

We also produced traverse image maps by back-projection of rover positions onto the image mosaics. Plate 1a shows the Spirit traverse (up to Sol 65) from Columbia Memorial Station uphill to the rim of Bonneville Crater. Plate 1b depicts the Opportunity traverse (up to Sol 192) from Eagle Crater, past the Anatolia region and Fram Crater, to Endurance Crater.

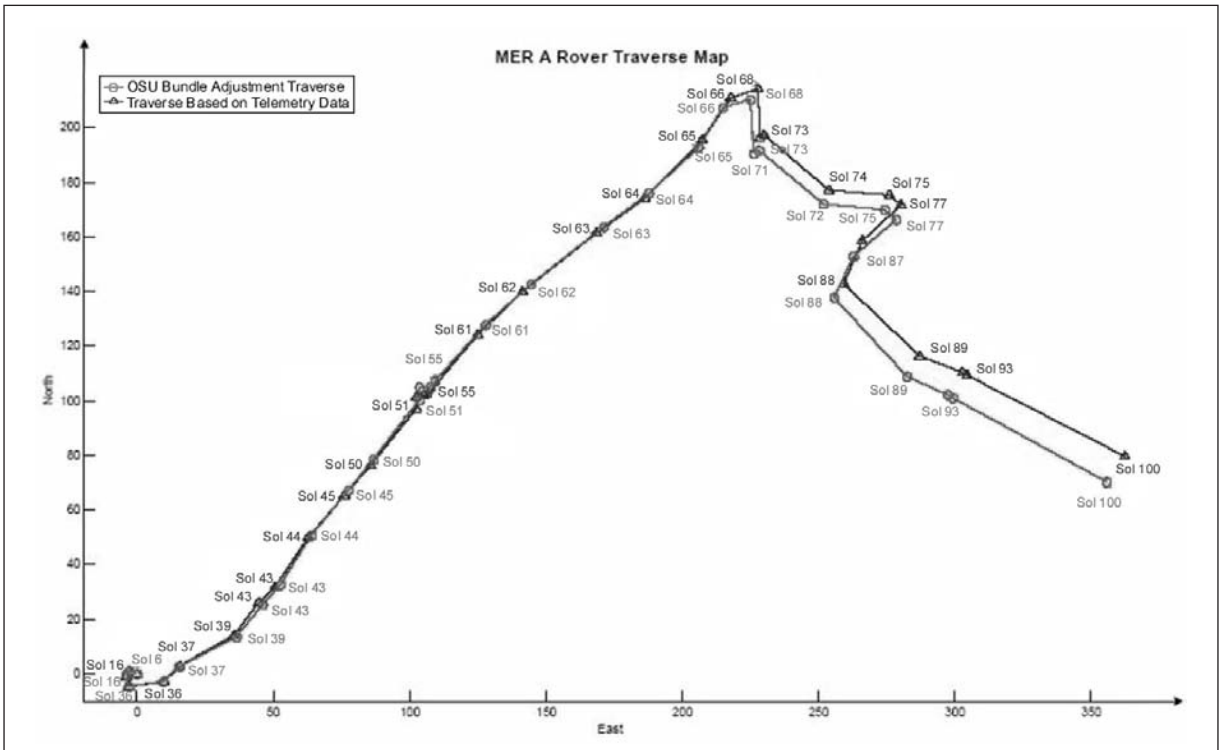

Figure 7. Spirit rover traverse map up to Sol 100 (line with triangular points from telemetry; line with circular points from bundle adjustment).

Topographic Mapping

Orthophoto Map Generation

Pancam and/or Navcam panoramas were often taken at the end of a drive where a new site frame was established. The average distance between two site frames at the Spirit Site (up to Sol 85) is about 36 m, with some of them over 100 m. Using these panoramic images, we generated orthophoto maps, each of which covers an area of 60 meters × 60 meters. Detailed rock locations, orientation, and map scale are all correctly presented in the orthophoto map. Consecutive orthophoto maps connected along the traverse describe the large-scale topography across the landing site.

The generation of orthophoto maps consists of five steps: (1) registration of interest points between intra-stereo images, (2) calculation of 3D locations of the matched interest points, (3) construction of a triangular irregular network (TIN) using the 3D matched points, (4) construction of a Digital Terrain Model (DTM as a grid) through an interpolation from the TIN, and (5) generation of the orthophoto map through projection between the images and the DTM.

Contrast and intensity distribution of the panoramic images generally change as cameras change direction due to different illumination conditions. A special method was developed to build balanced image sets for the orthophoto map by adjusting dynamic range and mean intensity over the inter-stereo tie points. If a bundle adjustment is performed, inter-stereo tie points suppress inconsistencies between adjacent stereo pairs and, thus, a seamless (subpixel inconsistency) orthophoto map can be produced. Figure 9 shows an orthophoto map of Laguna Hollow on Sol 45 with a resolution of 1 cm.

Vertical Profiles

In addition to local DTMs of orthophoto map sizes, a vertical profile was generated and expanded as each rover traversed in order to illustrate the terrain relief along the rover traverse. The horizontal position and elevation information are from the results of the bundle adjustments. Figure 10 shows the Spirit vertical profile up to Sol 214 when the rover reached the Columbia Hills region. The horizontal axis of the figure is the traveled distance from the lander; the vertical axis depicts elevation (scaled). Again, the line with triangular points is the profile computed from telemetry data, and the line with circular points shows the BA result. The accumulated elevation difference is 15.8 m over a traveled distance of 3.2 km. This difference may be attributed to wheel slippage and IMU drift.

Crater Mapping

Craters are one of the most topographically important features of the Spirit and Opportunity sites. The rovers collected a large amount of data at the Bonneville, Missoula, and Lahontan Craters (Spirit), as well the Eagle, Fram, and Endurance Craters (Opportunity). As Opportunity landed inside Eagle Crater (22 meters in diameter), it was consequently mapped very well by using the ground images collected almost at the center of the crater. As Fram Crater is small (7 m diameter), a partial Navcam panorama taken on the rim was able to cover the crater and build the DTM. Among the rest of the craters for which topographic data processing is pending, Endurance Crater is of greatest importance and interest. Opportunity spent 111 sols (up to Sol 206) around and inside the crater, whose diameter is about 156 m and depth is around 20 m. Two Pancam panoramas (color, three tiers) were taken on the rim: one on Sol 97 (west, Site 2002, 48 stereo pairs) and one on Sol 122 (southeast, Site 2809, 81 stereo pairs) (Plate 1c). For BA and crater mapping, we internally refer to the first panorama as P2002 and the second as P2809.

P2002 provides details of the west side of the crater, while P2809 better describes the southeast side. The logical

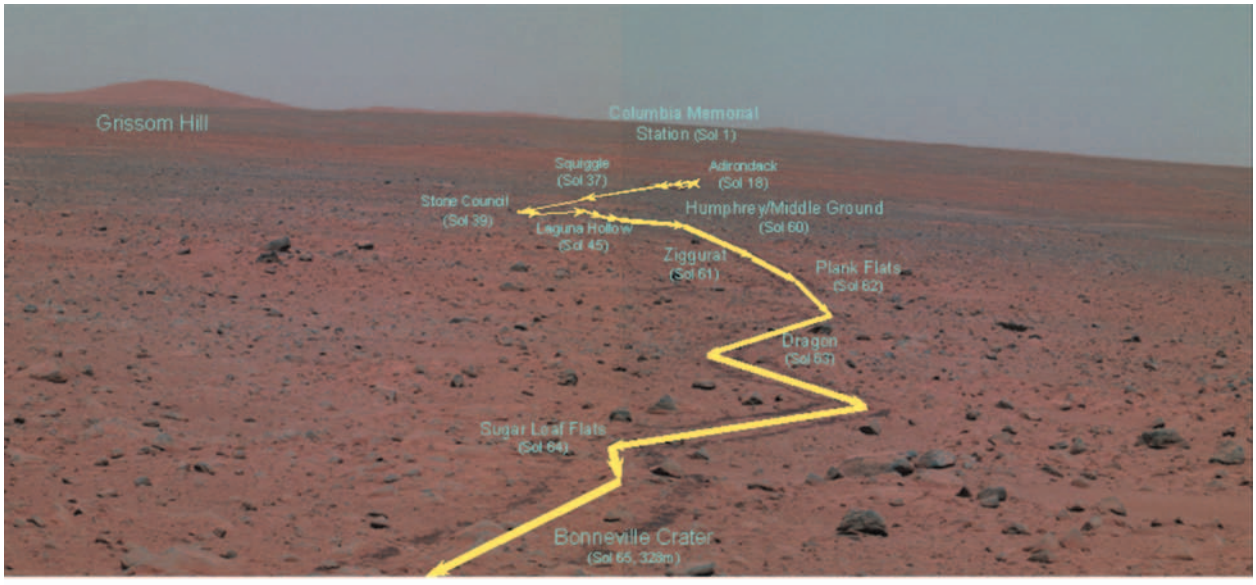

(a)

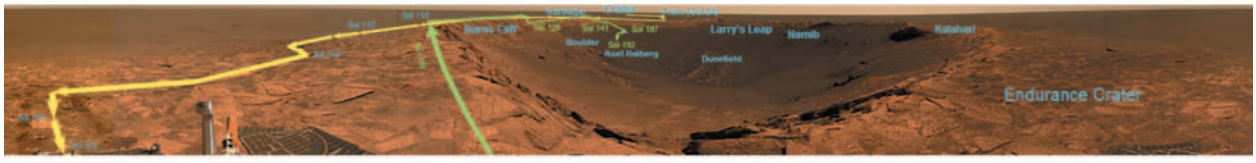

(b)

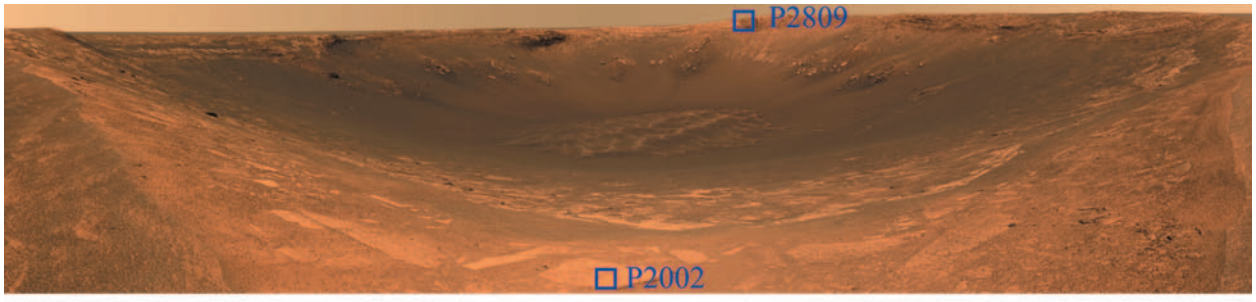

(c)

method for crater mapping is to incorporate both panoramas. Without correction, however, rover localization errors created inconsistencies of 6.7, 16.3, and 1.1 meters in *X*, *Y*, and *Z*, respectively, between the two panoramas as computed from 185 cross-site tie points (Figure 11a). The average inconsistency in the image space is 125 pixels. To perform unified crater mapping, a bundle adjustment of both panoramas was carried out. This BA resulted in much reduced differences of 2.1, 2.1, and 0.3 meters in 3D and 18 pixels in the images (Figure 11b).

Mapping topographic details of the 156 meter Endurance Crater using the two available panoramas is a challenge because the effective measured range from Pancam stereo images is only about 80 m. The most difficult parts of the crater for mapping based on the panorama configuration are the crater bottom and the north crater wall. An additional Pancam panorama was acquired at a rover location close to the bottom of the crater to cover the extra difficult areas of the crater.

We first generated individual terrain maps from P2002 and P2809 separately to provide an approximate model. After BA, we then built a crater DTM using both panoramas. Near P2002 (Plate 1c), 3D ground points derived from P2002 were used to provide details of the west wall area. Similarly, ground points from P2809 provide details of the southeast wall. The rest of the crater was mapped using ground points computed from both panoramas. In total, there are 43,941 ground points from P2002 and 107,085 ground points from P2809 used for crater mapping. An orthophoto map and a contour map of Endurance Crater are presented in Figure 12. A 3D perspective display of the DTM is shown in Figure 13.

Mapping with Orbital Data

Athena team members at the U.S. Geological Survey have used a variety of orbital image data to produce topographic models of the landing sites. These models have been useful in mission operations and planning in a variety of ways.

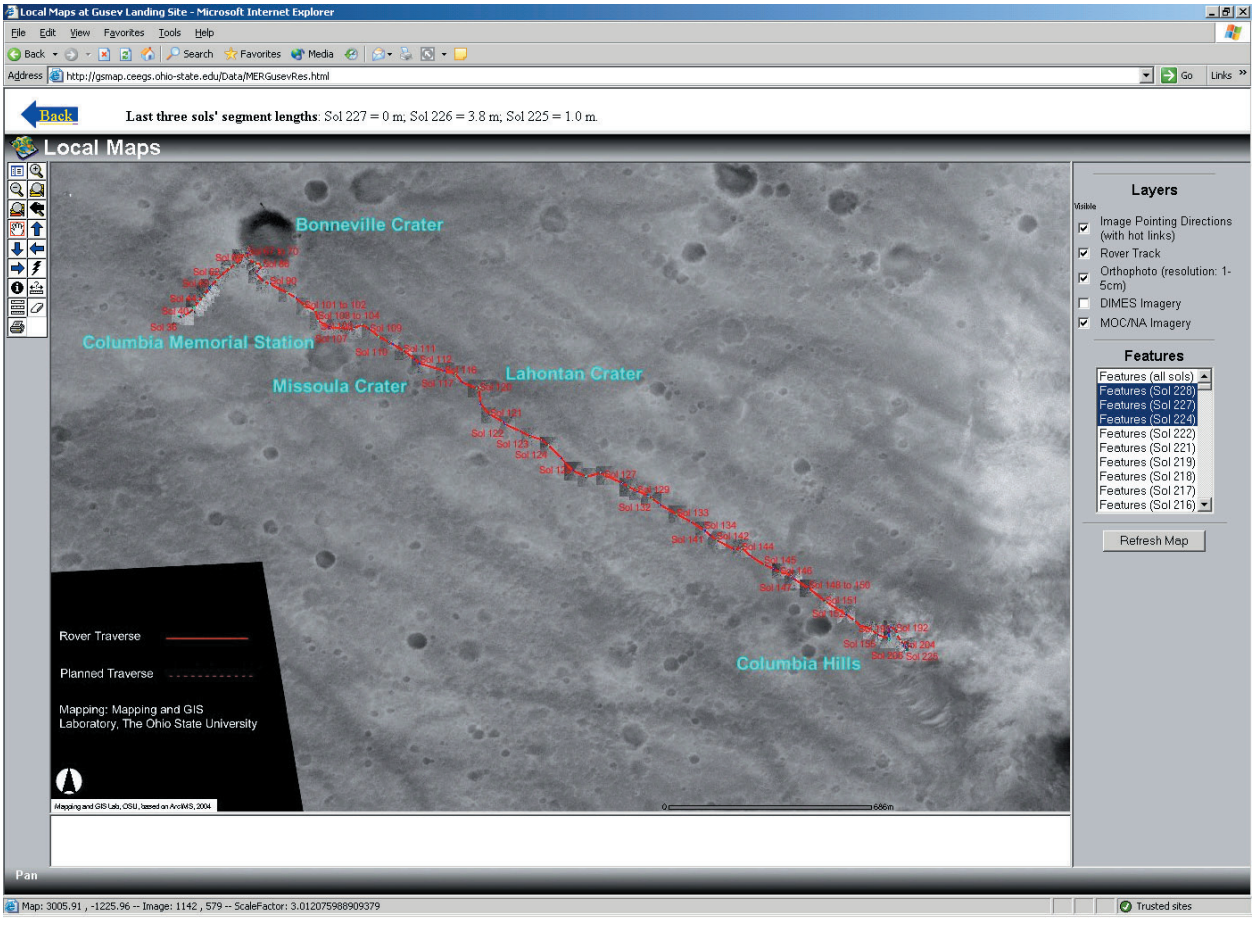

(d)

Plate 1. (a) Spirit rover traverse image map, uphill to Bonneville Crater on Sol 65; (b) Opportunity rover traverse image map up to Sol 192 (images taken on Sol 122); (c) Pancam panorama of Endurance crater at site 2002 with two site positions marked; and (d) Interface of the web GIS for accessing Spirit traverse information and local topographic products.

The capability for stereo mapping with images from the MOC NA camera (Malin *et al.*, 1992; Malin and Edgett, 2001) using SOCET SET® commercial photogrammetric software (Miller and Walker, 1993; 1995) in conjunction with the USGS cartographic software ISIS (Eliason, 1997; Gaddis *et al.*, 1997; Torson and Becker, 1997) was developed in 2001 and was used over the next several years to produce DTMs of representative terrains in candidate MER landing sites from which surface slope hazards could be estimated (Kirk *et al.*, 2003). These roughness estimates were an important input to the selection of the Gusev Crater and Meridiani Planum landing sites (Golombek *et al.*, 2003). Unfortunately, although the high resolution of the MOC NA images (approximately 3 m for the majority of images acquired with 2 × 2 pixel averaging) results in very high quality, 10 m post DTMs, the small size of the images means that overlapping images suitable for stereo analysis are relatively rare (Kirk *et al.*, 2004). Even in the selected MER sites, which were targeted repeatedly by MOC, stereo coverage is not continuous but consists of isolated terrain samples, and neither MER spacecraft landed in an area for which stereo coverage existed beforehand. An oblique image of the Spirit landing point giving useful stereo convergence in conjunction with earlier nadir images was obtained in January 2004, but the continuous pitch rotation of the spacecraft during acquisition of this image (CPROTO imaging mode) cannot be modeled with the existing SOCET SET® sensor model. We are currently working with BAE Systems to modify the software to enable such images to be used. The dearth of MOC stereo coverage led us to apply a novel technique of albedo correction followed by shape-from-shading for mapping the landing zones with 2001 Mars Odyssey THEMIS infrared images (Christensen *et al.*, 1999), as described in a companion paper by Kirk *et al.* (2005). The DTM resolution obtained by this means is on the order of 100 m.

Useful MOC stereo coverage was, however, available for a region near the MER-A landing point that was ultimately explored by the Spirit rover. A nadir image (E03-00012) of the Columbia Hills and a partly saturated oblique image (E16-01962) with significant changes in the surface appearance caused by dust devil activity were identified prior to landing. The poor quality of the second image precluded the use of automatic stereo matching, but a useful DTM of part of the Hills was obtained by manual editing. An unsaturated oblique image (R02-00357) in which the surface appearance better resembles the nadir image was subsequently identified and a 10 m/post DTM was generated by automatic matching with only localized manual editing. This dataset was used

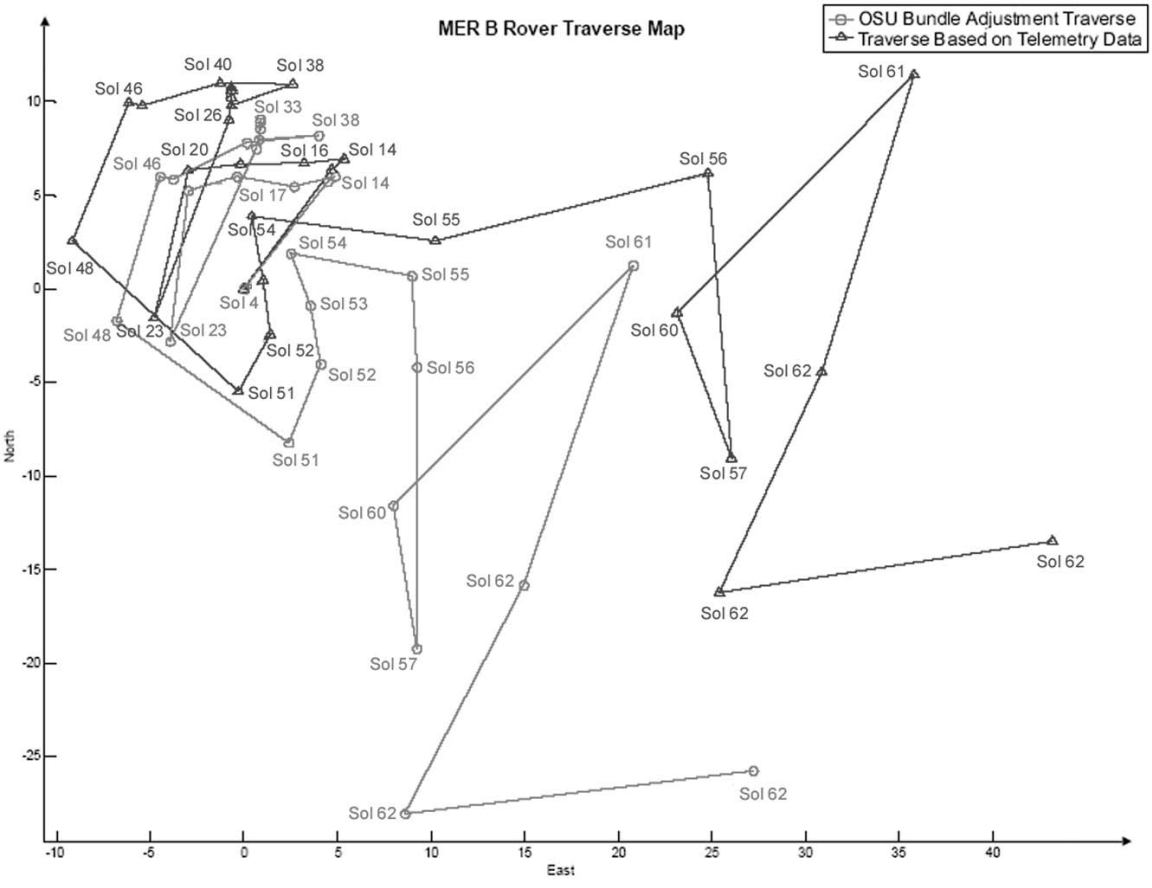

Figure 8. Opportunity rover traverse map (line with triangular points from telemetry; line with circular points from bundle adjustment).

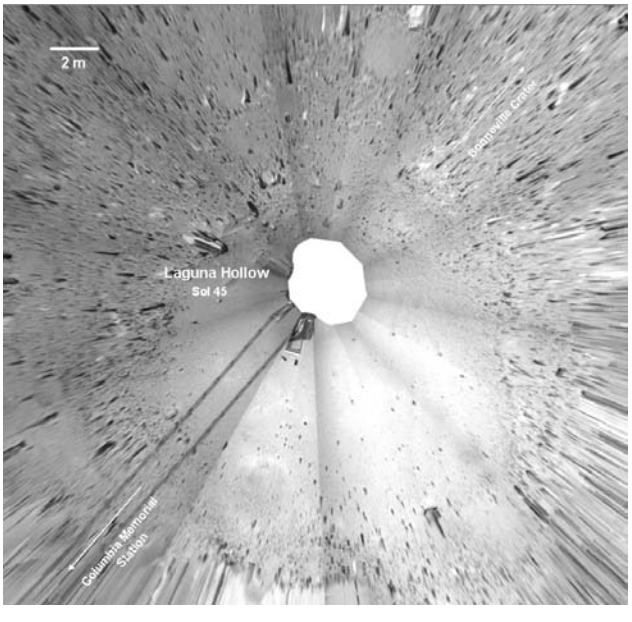

Figure 9. Spirit orthophoto map of Laguna Hollow at Site 9 on Sol 45 (60 m × 60 m, 1 cm/pixel).

in several ways in planning the operations of the Spirit rover. First, perspective views were helpful in clarifying stratigraphic relations in the hills and hence in identifying promising locations for the rover to sample the full geologic diversity of the area. Second, quantitative slope estimates derived from the DTM were compared with the rover performance in order to design a traverse that could reach the interest points safely. Finally, line-of-sight calculations were performed from a number of locations in and near the hills to the Sun, to the orbiting MGS and Odyssey spacecraft, and to other points on the ground. These calculations allowed mission planners to evaluate the favorability of different locations and traverse plans from the point of view of available solar power, communications with Earth, and maximization of the area imaged and studied by the rover, respectively. A MOC stereo pair (images R14-00021 and R14-01689) of the planned traverse of the Opportunity rover as it moved south from the Endurance Crater was recently acquired and is being used for similar purposes.

Applications

The OSU Mapping and GIS Laboratory uses its proprietary "MarsMapper" software system to generate mapping products and to provide accurate bundle-adjusted rover localization information for both rovers, which are organized and disseminated to mission scientists and engineers through a

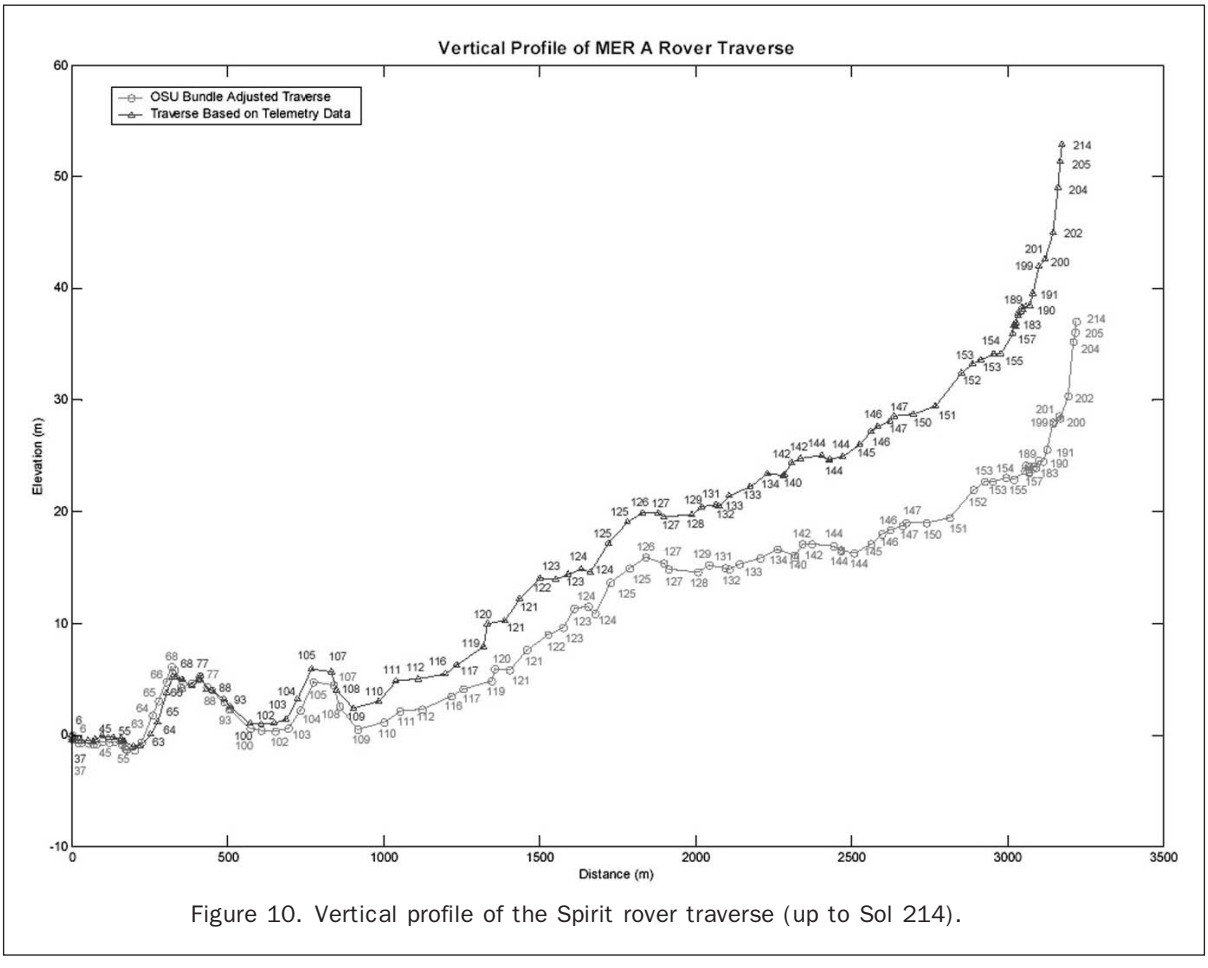

Figure 10. Vertical profile of the Spirit rover traverse (up to Sol 214).

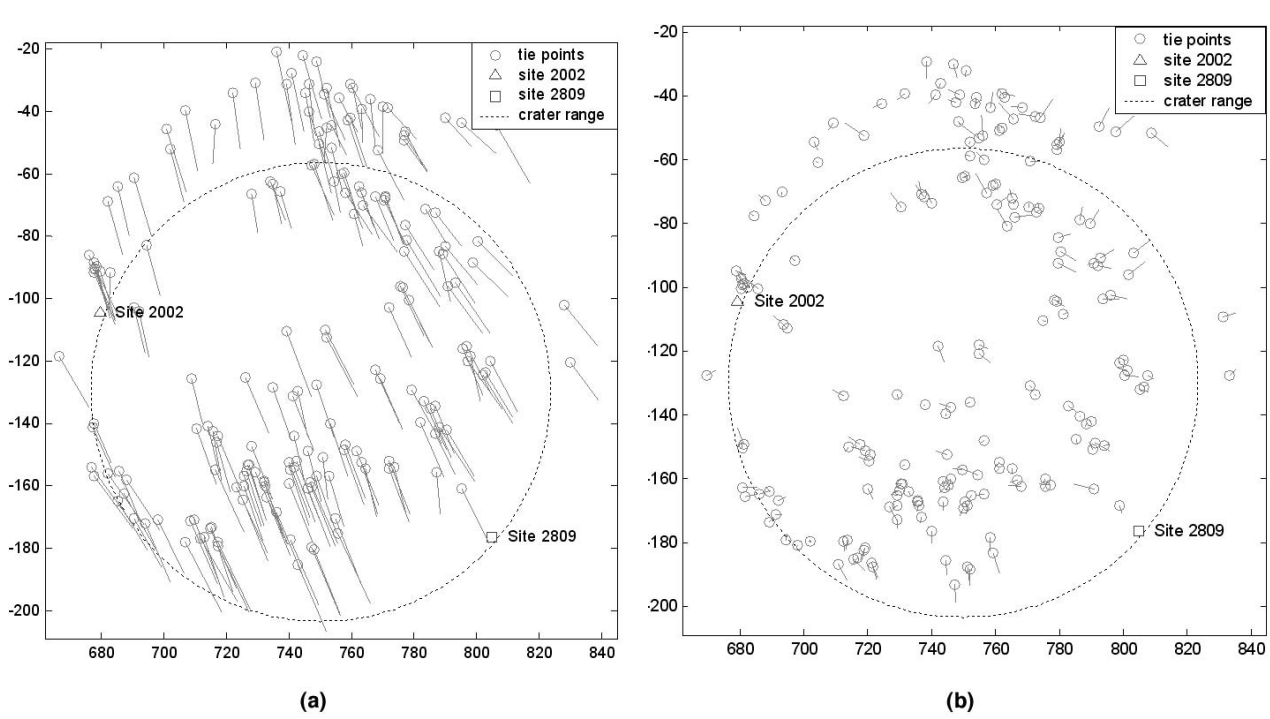

Figure 11. Difference of cross-site tie points between site 2002 and 2809: (a) before adjustment, and (b) after adjustment.

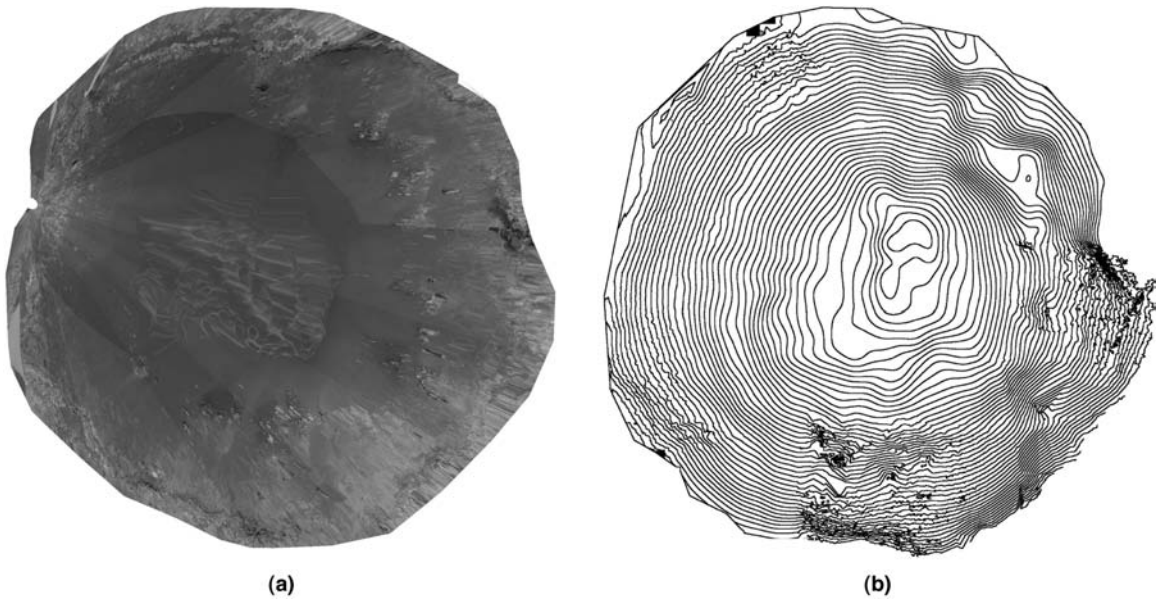

Figure 12. (a) Orthophoto map and (b) contour map of Endurance Crater.

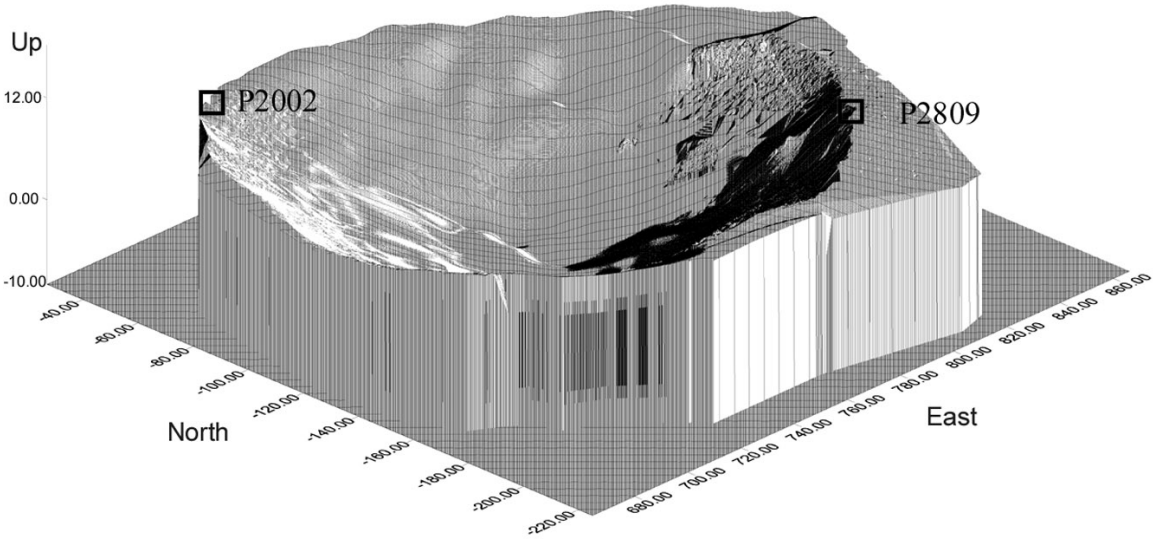

Figure 13. 3D perspective meshed grid of Endurance Crater.

web-based GIS developed for this mission. These products include up-to-date orthophoto maps, DTMs, crater models, traverse image maps, contour maps, georeferenced DIMES images, rover traverse graphics and positions (coordinates), as well as other special products requested by scientists and engineers. During mission operations, this web GIS has constantly tracked and corrected rover positions, and provided updated mapping information including appropriate MOC NA, DIMES, and ground orthophoto images (Plate 1d).

Accurate localization conveys multiple benefits, both for planning activities on the tactical time scale (sol by sol) and also for the long-term objective of creating a robust data set for the entire mission. It allowed Spirit to achieve the maximum number of observations possible without compromising the driving schedule.

An important goal of geologic analysis of rover data is development of "ground truth" for orbital remote sensing data sets. In practice, this involves simple correlation of characteristics identified in orbital data with these characteristics as seen at the surface. Localization of the rover within orbital data sets is essential to this correlation. During the traverse across the plains from Bonneville Crater to the Columbia Hills (Plate 1d), several significant correlations were identified including the surface manifestations of apparent radial differences in impact crater ejecta (Grant *et al.*, 2004; Crumpler *et al.*, 2004) and surface characteristics of variations in thermal characteristics. Traverse localization indicated that Spirit twice crossed these divisions of "continuous ejecta" and "discontinuous ejecta" on the Bonneville, Missoula, and Lahontan Craters. In addition, the corresponding variations in

clast size distribution across the ejecta sheets were possible since localization enabled a site-by-site mapping of observed distributions from rover observations with positions within the ejecta sheets.

Variations in thermophysical properties in THEMIS data implied possible differences in the distribution of clasts and soils along the traverse. Combining detailed locations of observation sites with corresponding positions within the orbital data implied that subtle differences in small impact craters and local topography were likely responsible for influencing local fines accumulation.

Furthermore, systematic surveys on Spirit of wind-related features have been useful for characterizing transportation and organization of sand and dust on the floor of Gusev Crater (Greeley *et al.*, 2004). By providing a consistent frame of reference, localization has enabled an accurate assessment of the orientation of wind-related features that are separated by more than 3 km.

Conclusions

The above is a summary of the achievements of localization and topographic mapping efforts of several groups of the MER 2003 mission (by Sol 225 for Spirit and Sol 206 for Opportunity). Successful localization of the landers within seven sols after landing at the Gusev Crater and Meridiani Planum landing sites and verification by MOC NA orbital images together supported science planning in the early stages of surface operations. Visual odometry has been used frequently to give accurate rover locations when driving toward a target (mostly in approaching sols with shorter distances), and has demonstrated its ability to overcome significant slippages such as those experienced by the MER rovers. Incremental bundle adjustment, on the other hand, built a global image network of each rover traverse to reduce accumulated rover position errors, and was able to correct position errors as large as 18.7 m over a distance of 91.4 m (20.5 percent). The improved visual odometry and bundle-adjustment results and orbital images ensured that the topographic mapping products of the landing sites were generated with a very high quality. The localization and topographic mapping results, including processed images, maps, DTMs, and rover traverses, have been utilized for strategic planning and tactical operations and have benefited a large number of science application areas.

The majority of the instruments onboard both rovers were still healthy as of 01 October 2004, and they continue to explore the Martian surface. We expect to report further localization and topographic mapping results to be achieved in the remaining time of the mission and from post-mission data processing.

Acknowledgments

Funding of the research by the Mars Exploration Program of NASA is acknowledged. Thanks to Irene Tesfai of OSU for proofreading several versions of the manuscript.

References

Arvidson, R.E., R.C. Anderson, P. Bartlett, J.F. Bell, III, D. Blaney, P.R. Christensen, P. Chu, L. Crumpler, K. Davis, B.L. Ehlmann, R. Fergason, M.P. Golombek, S. Gorevan, J.A. Grant, R. Greeley, E.A. Guinness, A.F.C. Haldemann, K. Herkenhoff, J. Johnson, G. Landis, R. Li, R. Lindemann, H. McSween, D.W. Ming, T.Myrick, L. Richter, F.P. Seelos, IV, S.W. Squyres, R.J. Sullivan, A. Wang, and J. Wilson, 2004. Localization and physical properties experiments conducted by Spirit at Gusev Crater, *Science, Special Issue on MER 2003 Mission*, 305(5685):821–824 (doi: 10.1126/science.1099922).

Biesiadecki, J.J., and M.W. Maimone, 2005. The Mars Exploration Rover surface mobility flight software: Driving ambition, *IEEE Aerospace Conference*, Big Sky, Montana, 05–12 March, Vol. 5.

Christensen, P.R., B.M. Jakosky, H.H. Kieffer, M.C. Malin, H.Y. McSween, Jr., K. Nealson, G. Mehall, S. Silverman, and S.Ferry, 1999. The Thermal Emission Imaging System (THEMIS) instrument for the 2001 Orbiter, *Lunar Planetary Science, XXX*, Abstract #1470, Lunar and Planetary Institute, Houston, Texas (unpaginated CD-ROM).

Crumpler, L., In Review. MER: Geological traverse science by the Spirit rover in the Gusev plains, Mars, *Nature, Special Issue of Mars Exploration Rover Mission*.

Di, K., and R.Li, 2004. CAHVOR camera model and its photogrammetric conversion for planetary applications, *Journal of Geophysical Research, Planets*, 109(E4):E04004 (doi: 10.1029/2003JE002199).

Di, K., F. Xu, R. Li, L. Matthies, C. Olson, 2002. High precision landing site mapping and rover localization by integrated bundle adjustment of MPF surface images, *International Archives of the Photogrammetry, Remote Sensing and Spatial Information Sciences (IAPRS)*, 34(4):733–737.

Eliason, E., 1997. Production of digital image models (DIMs) using ISIS, *Lunar and Planetary Science*, *XXVIII*, 331–332, Lunar and Planetary Institute, Houston, Texas.

Gaddis, L., J. Anderson, K. Becker, T. Becker, D. Cook, K. Edwards, E. Eliason, T. Hare, H. Kieffer, E.M. Lee, J. Mathews, L. Soderblom, T. Sucharski, and J. Torson, 1997. An overview of the Integrated Software for Imaging Spectrometers (ISIS), *Lunar and Planetary Science*, *XXVIII*, 387–388, Lunar and Planetary Institute, Houston, Texas.

Greeley, R., S.W. Squyres, R.E. Arvidson, P. Bartlett, J.F. Bell, III, D. Blaney, N.A. Cabrol, J. Farmer, B. Farrand, M.P. Golombek, S.P. Gorevan, J.A. Grant, A.F.C. Haldemann, K.E. Herkenhoff, J. Johnson, G. Landis, M.B. Madsen, S.M. McLennan, J. Moersch, J.W. Rice, Jr., L. Richter, S. Ruff, R.J. Sullivan, S.D. Thompson, A. Wang, C.M. Weitz, and P. Whelley, and the Athena Science Team, 2004. Wind-Related processes detected by the Spirit rover at Gusev Crater, *Science*, 305(5685):810–813.

Golombek, M.P., J.A. Grant, T.J. Parker, D.M. Kass, J.A. Crisp, S.W. Squyres, A.F.C. Haldemann, M. Adler, W.J. Lee, N.T. Bridges, R.E. Arvidson, M.H. Carr, R.L. Kirk, P.C. Knocke, R.B. Roncoli, C.M. Weitz, J.T. Schofield, R.W. Zurek, P.R. Christensen, R.L. Fergason, F.S. Anderson, J.W. Rice, Jr., 2003. Selection of the Mars Exploration Rover landing sites, *Journal of Geophysical Research, Planets*, 108(E12):8072 (doi: 10.1029/2003JE002074).

Golombek, M., and T. Parker, 2004. Lander localization, *MER Project Memorandum* (one for Spirit, one for Opportunity), JPL/NASA.

Grant, J.A., R. Arvidson, J.F. Bell, III, N.A. Cabrol, M.H. Carr, P. Christensen, L. Crumpler, D.J. Des Marais, B.L. Ehlmann, J. Farmer, M. Golombek, F.D. Grant, R. Greeley, K. Herkenhoff, R. Li, H.Y. McSween, D.W. Ming, J. Moersch, J.W. Rice, Jr., S Ruff, L. Richter, S. Squyres, R. Sullivan, and C. Weitz, 2004. Surficial deposits at Gusev Crater along Spirit rover traverses, *Science*, 305(5685):807–810.

Guinn, J.R., and T.A. Ely, 2004. Preliminary Results of Mars Exploration Rover in situ radio navigation, Presentation, 14th AAS/AIAA Space Flight Mechanics Meeting, AAS 04–270, Maui, Hawaii, 08–12 February.

Johnson, A., 2004. MER-B DIMES localization, Presentation, JPL/NASA, 30 January, Pasadena, California.

Kirk, R.L., E. Howington-Kraus, B. Redding, D. Galuszka, T.M. Hare, B.A. Archinal, L.A. Soderblom, and J.M. Barrett, 2003. High-resolution topomapping of candidate MER landing sites with Mars Orbiter Camera Narrow-Angle images, *Journal of Geophysical Research*, 108(E12):8088 (doi: 10.1029/2003JE002131).

Kirk, R.L., E. Howington-Kraus, T. Hare, R. Soricone, K. Ross, L. Weller, M. Rosiek, B. Redding, D. Galuszka, and B.A. Archinal, 2004. High-resolution topo mapping of Mars: Life after MER site selection, *Lunar and Planetary Science, XXXV*, Abstract No. 2046, Lunar and Planetary Institute, Houston (unpaginated CD-ROM).

Kirk, R.L., Soderblom, L.A., Cushing, G., and Titus, T., 2005. Joint analysis of Mars Odyssey THEMIS visible and infrared images: A "magic airbrush" for qualitative and quantitative topography, *Photogrammetric Engineering & Remote Sensing*, 71(10).

Li, R., F. Ma, F.Xu, L.H. Matthies, C.F. Olson, and R.E. Arvidson, 2002. Localization of Mars rovers using descent and surface-based image data, *Journal of Geophysical Research, Planets, FIDO Special Issue* (R.E. Arvidson, editor), 107(E11): FIDO 4.1–4.8.

Li, R., K. Di, and F. Xu, 2003. Automatic Mars landing site mapping using surface-based images, ISPRS WG IV/9: Extraterrestrial Mapping Workshop on Advances in Planetary Mapping, 22 March, Houston, Texas, URL: http://www.lpi.usra.edu/meetings/lpsc2003/lpsc2003.download.html (last date accessed: 29 June 2005).

Li, R., K. Di, L.H. Matthies, R.E. Arvidson, W.M. Folkner, and B.A. Archinal, 2004a. Rover localization and landing site mapping technology for 2003 Mars Exploration Rover mission, *Photogrammetric Engineering & Remote Sensing*, 70(1):77–90.

Li, R., K. Di, L. Matthies, M. Maimone, R.E. Arvidson, L. Crumpler, F. Xu, J. Wang, X. Niu, C. Serafy, D. Ming, L. Richter, D. Des Marais, M. Golombek, S. Squyres, A. Johnson, J. Bell, J.N. Maki, M. Malin, T. Parker, L. Edwards, M. Sims, A. Wang, J. Garvin, L. Soderblom, and the Athena Science Team, 2004b. Topographic mapping and rover localization in MER 2003 mission landing sites, Poster, AGU Joint Assembly, Montréal, 17–21 May.

Malin, M.C., G.E. Danielson, A.P. Ingersoll, H. Masursky, J. Veverka, M.A. Ravine, and T.A. Soulanille, 1992. Mars Observer Camera, *Journal of Geophysical Research, 97*:7699–7718, 1992.

Malin, M.C., and K.S. Edgett, 2001. Mars Global Surveyor Mars Orbiter Camera: Interplanetary cruise through primary mission, *Journal of Geophysical Research*, 106(E10):23,429–23,570.

Malin, M., 2004. MOC cPROTO and ROTO images with Spirit and Opportunity landers, URL: http://www.msss.com/mer_mission/index.html, Malin Space Science Systems, San Diego, California, (last date accessed: 29 June 2005).

Miller, S.B., and A.S. Walker, 1993. Further developments of Leica digital photogrammetric systems by Helava, *ACSM/ASPRS Annual Convention and Exposition Technical Papers*, 3, 256–263.

Miller, S.B., and A.S. Walker, 1995. Die Entwicklung der digitalen photogrammetrischen Systeme von Leica und Helava, *Zeitschrift für Photogrammetric und Fernerkundung, 1*(95):4–16.

Norris, J.S., M.W. Powell, M.A. Vona, P.G. Backes, and J.V. Wick, 2004. Mars Exploration Rover Operations with the Science Activity Planner, NASA Inventions and Contributions Board, URL: http://icb.nasa.gov/SWOY2004/SAP-SOYA-Presentation.ppt (last accessed 29 June 2005).

Olson, C.F., L.H. Matthies, M. Schoppers, and M.W. Maimone, 2003. Rover navigation using stereo ego-motion, *Robotics and Autonomous Systems*, 43(4):215–229.

Parker, T., M. Malin, M. Golombek, T. Duxbury, A. Johnson, J. Guinn, T. McElrath, R. Kirk, B. Archinal, L. Soderblom, R. Li, the MER Navigation Team, and the Athena Science Team, 2004. Localization, localization, localization, Report, 35th Lunar and Planetary Science Conference, League City, Texas, 15–19 March, 2 pages.

Squyres, S.W., R.E. Arvidson, E.T. Baumgartner, J.F. Bell, III, P.R. Christensen, S. Gorevan, K.E. Herkenhoff, G. Klingelhöfer, M.B. Madsen, R.V. Morris, R. Rieder, and R.A. Romero, 2003. Athena Mars rover science investigation, *Journal of Geophysical Research*, 108(E12):8062 (doi: 10.1029/2003JE002121).

Squyres, S.W., R.E. Arvidson, J.F. Bell, III, J. Brückner, N.A. Cabrol, W. Calvin, M.H. Carr, P.R. Christensen, B.C. Clark, L. Crumpler, D.J. Des Marais, C. d'Uston, T. Economou, J. Farmer, W. Farrand, W. Folkner, M. Golombek, S. Gorevan, J.A. Grant, R. Greeley, J. Grotzinger, L. Haskin, K.E. Herkenhoff, S. Hviid, J. Johnson, G. Klingelhöfer, A. Knoll, G. Landis, M. Lemmon, R. Li, M.B. Madsen, M.C. Malin, S.M. McLennan, H.Y. McSween, D.W. Ming, J. Moersch, R.V. Morris, T. Parker, J.W. Rice, Jr., L. Richter, R. Rieder, M. Sims, M. Smith, P. Smith, L.A. Soderblom, R. Sullivan, H. Wänke, T. Wdowiak, M. Wolff, and A. Yen, 2004a. The Spirit rover's Athena science investigation at Gusev Crater, Mars, *Science, Special Issue on MER 2003 Mission (Spirit)*, 305(5685):794–799.

Squyres, S.W., J.P. Grotzinger, R.E. Arvidson, J.F. Bell III, P.R. Christensen, B.C. Clark, J.A. Crisp, W.H. Farrand, K.E. Herkenhoff, J.R. Johnson, G. Klingelhöfer, A.H. Knoll, S.M. McLennan, H.Y. McSween, R.V. Morris, J.W. Rice, Jr., R. Rieder, and L.A. Soderblom, 2004b. In situ evidence for an ancient aqueous environment on Meridiani Planum, Mars, *Science, Special Issue on MER 2003 Mission (Opportunity)*, 306(5702):1709–1714 (doi: 10.1126/science.1104559).

Torson, J., and K. Becker, 1997. ISIS: A software architecture for processing planetary images, *Lunar and Planetary Science, XXVIII*, 1443–1444, Lunar and Planetary Institute, Houston.

Xu, F., K. Di, R. Li, L. Matthies, and C. Olson, 2002. Automatic feature registration and DEM generation for Martian surface mapping, *International Archives of the Photogrammetry, Remote Sensing and Spatial Information Sciences (IAPRS)*, 34(2):549–554.